Available online at www.sciencedirect.com

ScienceDirect

journal homepage: http://www.elsevier.com/locate/acme

Original Research Article

Seismic behavior of concrete-filled double-skin steel tube/moment-resisting frames with beam-only-connected precast reinforced concrete shear walls

Yi Hu, Junhai Zhao *, Dongfang Zhang, Yanxiong Chen

School of Civil Engineering, Chang'an University, Xi'an 710061, China

ARTICLE INFO

Article history:
Received 28 December 2018
Accepted 26 April 2019
Available online 28 May 2019

Keywords:
Concrete-filled double-skin steel tube
Composite structures
RC shear walls
Prefabricated structures
Seismic behavior

ABSTRACT

Concrete-filled double-skin steel tube (CFDST) attracts attention from researchers for it exhibits high strength, good ductility and energy dissipation capacity. In this paper, CFDST frame with beam-only-connected precast reinforced concrete shear wall system is proposed, and all the joints used high-strength bolt connection to realize fully-prefabricated construction. Three specimens were tested to obtain the seismic performance and cooperative mechanism of such proposed systems, and the contribution of beam-only-connected precast reinforced concrete shear wall (BRW) was quantified by comparing the results of these specimens. The results show that: (1) the BRW cooperated well with the CFDST frames, and it significant enhanced the lateral stiffness and strength of the CFDST frame; (2) all specimens tolerated more than 4% inter-story drift ratio, indicating that the specimens have good lateral deformation capacity; (3) the specimen with two pieces of BRW (BF-BRW-B) exhibited better ductility ratio by comparing with the specimen without BRW (BF) and with only one piece of BRW (BF-BRW-A); (4) relative brittle failure was occurred on the BRW in BF-BRW-A due to the shear force, which resulted in significant strength degradation and ductility reduction of the specimen, but two BRWs in BF-BRW-B could mitigate such situations. Lastly, equations were proposed to predict the lateral resistance of the test specimens.

1. Introduction

In the past several decades, more and more high-rise buildings have been constructed all around the world, especially in the metropolises. Thus new structural systems with better performance and lower cost were desired for the engineers, and concrete-filled steel tube (CFST) was proposed for its high strength and stiffness, good ductility and energy dispassion capacity. In the recent decade, the concrete-filled double-skin steel tube (CFDST) was proposed because of its better performance, fire and corrosion resistances and less self-

* *Corresponding author.*
E-mail addresses: hyi_1991@163.com (Y. Hu), zhaojh@chd.edu.cn (J. Zhao).
https://doi.org/10.1016/j.acme.2019.04.009

weight [1]. A CFDST component includes an outer tube and an inner tube, the inner tube could provide more restraining force for the infilled concrete and provide vertical and lateral resistance if the outer tube was damaged. Many researchers conducted experimental and analytical investigations on the CFDST components, such as its performance of CFDST columns subjected to cyclic bending loads [2], the theoretical calculation for compressive bearing capacity of CFDST columns [3], the numerical modeling method for compression performance prediction of CFDST columns [4], the performance of CFDST columns subjected to pure torsion load [5], the bending-shear performance of CFDST columns [6], and the numerical modeling method for performance simulation of CFDST short columns [7]. The mentioned advantages were demonstrated in these investigations, and such findings promote further applications of CFDST frame structures in engineering practice.

Due to the advantages of CFDST components, the performance of CFDST structures is attracting researchers' attention, especially for the CFDST frame structures. Many researches have been conducted for CFST frames, including the numerical modeling method of concrete-filled SHS column frames [8], test research of CFT/BRB frame [9], the modeling method of the behavior of panel zone in CFST frame [10], the effects of modeling level selection for seismic fragility of CFST frame [11], the seismic behavior of CFST frames with semi-rigid connections [12], the cyclic behavior of CFST column to composite beam frame [13], and seismic performance of CFST frame with steel plate shear wall and composite steel plate shear wall [14]. It was found that the CFST frames exhibit high lateral resistance and energy dissipation capacity, however, the investigations on the CFDST frames are insufficient because of the different mechanical behavior between CFST and CFDST components. In recent years, Zhang et al. performed quasi-static tests on CFDST column-reinforced concrete (RC) beam joints [15] and CFDST column-steel beam joints [16], and aimed to investigate the seismic performance of CFDST in frame structures, it was found that the CFDST column-steel beam joints exhibit better performance, but the ductility of the joints was reduced due to fracture of weld connections. Hu et al. [17] developed a simplified numerical model for the CFDST frame buildings, and assessed the seismic risk of a case CFDST frame building, however, it was indicated that such proposed model was only verified by the test results of the joints, but not of the frame structure. Besides, a fully-prefabricated CFDST frame system was proposed, only high-strength bolts were used for the beam-to-column joints and the column-to-column joints. The seismic performance of the proposed frame system has been investigated, and comparative specimens with different types of construction details were also tested and analyzed [18].

In the regions with high seismicity, the lateral resistance and the lateral stiffness of the frame building are insufficient. To avoid large deformation and to ensure the safety of the frame buildings in strong earthquake regions, shear wall was proposed as a strengthen component that can be infilled into the frames, including steel plate shear wall (SPSW) and reinforced concrete (RC) shear wall. The shear walls could enhance the strength and stiffness of the frame building, and could reduce the collapse consequences of them due to earthquake, because the shear walls would become the second defense line of the frame structure [19]. Due to the good fire resistance and large lateral stiffness, the RC shear walls are commonly used in frame buildings, and the seismic performance of different types of RC shear walls has been investigated in literature, including the innovative seismic-resistant steel frame with RC infill walls [20], the steel frames with concrete sandwich panels [21] and the partially restrained steel frame-RC infill walls [22]. These types of RC shear walls are commonly connected with boundary columns and boundary beams. It was found that the shear force of the shear walls would transfer to the boundary frame and result in additional forces for the boundary columns, thus large section of columns was needed to resist the additional force derived by the shear walls, such finding was reported by many researchers [23–25]. Therefore, researches suggested that separating the RC shear walls from the boundary columns and the RC shear walls was connected only with the boundary beams, including the steel frame with separated RC infill walls [26] and the steel frame partially infilled with RC wall systems [27]. Generally, such suggestion was also proposed in SPSW and composite shear wall system, and this kind of shear wall was commonly named as beam-only-connected shear wall, including steel plate shear walls with beam-connected web plates [28], LYS and HYS steel plate shear walls connected to frame beams only [29], steel plate shear walls with composite columns and infill plate plates connected to beams only [30] and steel frame equipped with steel panel wall [31]. However, the beam-only-connected RC shear walls are scarcely investigated, especially in CFDST frames. If a RC shear wall infill frame structure encountered a severe earthquake, the damaged RC shear wall might not easy be repaired or retrofitted because most of the RC shear wall infill frame systems used the cast-in situ construction. Such construction was commonly used because few connecting technologies were proposed to realize fabricated connection between the boundary frames and the RC shear walls, especially for the steel frames with RC shear walls [27].

Therefore, this paper used high-strength bolts to connect the beam-only-connected RC shear wall (BRW) and the boundary CFDST frame to realize fabricated construction of this structural system. One CFDST frame specimen and two CFDST frame with BRW specimens were designed and tested. These specimens were designed in 1/2 reduced scale with single-story and single-bay. The failure mechanism and seismic performance of the test specimens were investigated and compared. The structural design method for lateral capacity prediction of the BRWs is also proposed and validated.

2. Experimental work

2.1. *Bare frame (BF) specimen*

A fully-prefabricated concrete-filled double-skin steel tube/moment-resisting frame (PCFDSF, this paper abbreviates it as BF) specimen was designed based on an actual concrete-filled steel tube frame structure, and such bare frame was used as a benchmark model in the test program of this paper. Due to the limitation of the test condition, the bare frame was scaled

down to 1:2-scaled size, and it was designed as single-bay and single-story. The total height and the story height of the bare frame were 1.62 m and 1.5 m, respectively. The bay length of the bare frame was 3.0 m. The bare frame was constructed by two concrete-filled double skin steel tube (CFDST) columns and a H-section steel beam. The CFDST column includes a square-section outer tube and a circular-section inner tube, and concrete was pulled into the space between the outer and inner tubes. The side length and the plate thickness of the outer tubes were 250 mm and 8 mm, respectively. The diameter and the plate thickness of the inner tubes were 133 mm and 6 mm, respectively. The section height, flange width, web thickness and flange thickness of the steel beam were 244 mm, 175 mm, 7 mm and 11 mm, respectively.

In this paper, a fully-prefabricated construction technology is proposed. Both the beam-to-column joints and the column-to-column joints were connected by high-strength bolts, and both of the novel splicing-type column-to-column connection and the novel block-strengthened connection are proposed, respectively.

The construction details and the dimensions of the proposed splicing-type connection are shown in Fig. 1 and Fig. 2, respectively. A single-story CFDST column in the BF specimen was divided into two parts: the upper half part (700 mm in height, Fig. 1(a)) and the bottom half part (700 mm in height, Fig. 1(b)). Four T-shape stiffeners and a splicing plate were welded around the inner tube in each part, and were connected with the outer tube of each part, as shown in Fig. 1 (a) and (b). These parts could be assembled in the factory, and the concrete was pulled into the space between the inner tube and the outer tube at this stage. Then these parts can be transformed to the construction site and can be connected by connecting the splicing plates, and a pair of U-shape encapsulation components were used to seal up the splicing regions, as shown in Fig. 1(c). The completed CFDST column is shown in Fig. 1(d).

The dimensions details of the proposed block-strengthened connection are shown in Fig. 3. Among the stiffeners, the cover plates and the blocks were used to strengthen the connections. As shown in Fig. 1(a), both of the stiffeners and the cover plates were welded with the upper half of the CFDST column in the factory. Then the steel beam was placed between the cover plates and was connected with these plates and CFDST column by high-strengthen bolts. The blocks were placed at the end of steel beam and were connected with the steel beam and CFDST column by high-strengthen bolts (Fig. 4).

2.2. *Beam-only-connected precast reinforced concrete shear wall*

Beam-only-connected precast reinforced concrete shear wall (BRW) is proposed to enhance the BF in the regions with severe earthquake. By comparing with the steel plate shear wall, the RC shear wall exhibits good fire-resistance and can be used as thermal-insulating wall. By changing the size and the numbers, the BRWs could provide transformable space for architecture requirements. In this paper, two BF-BRWs speci-

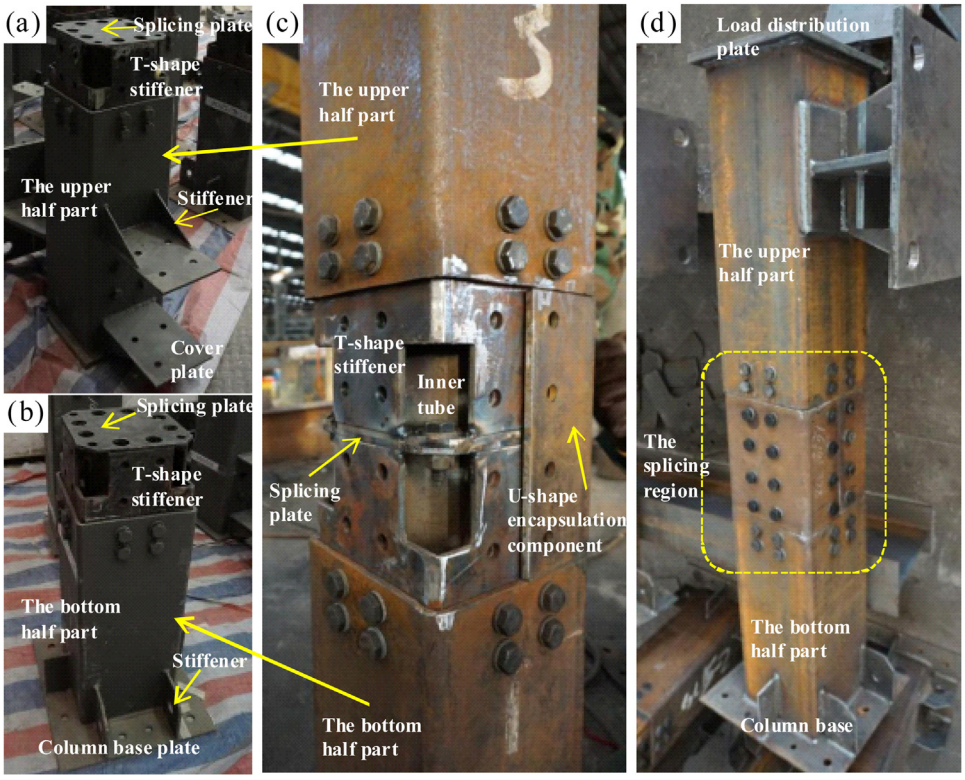

Fig. 1 – Spicing-type column-to-column joint (a. the upper half part; b. the bottom half part; c. details of column-to-column connection; d. the connected CFDST column).

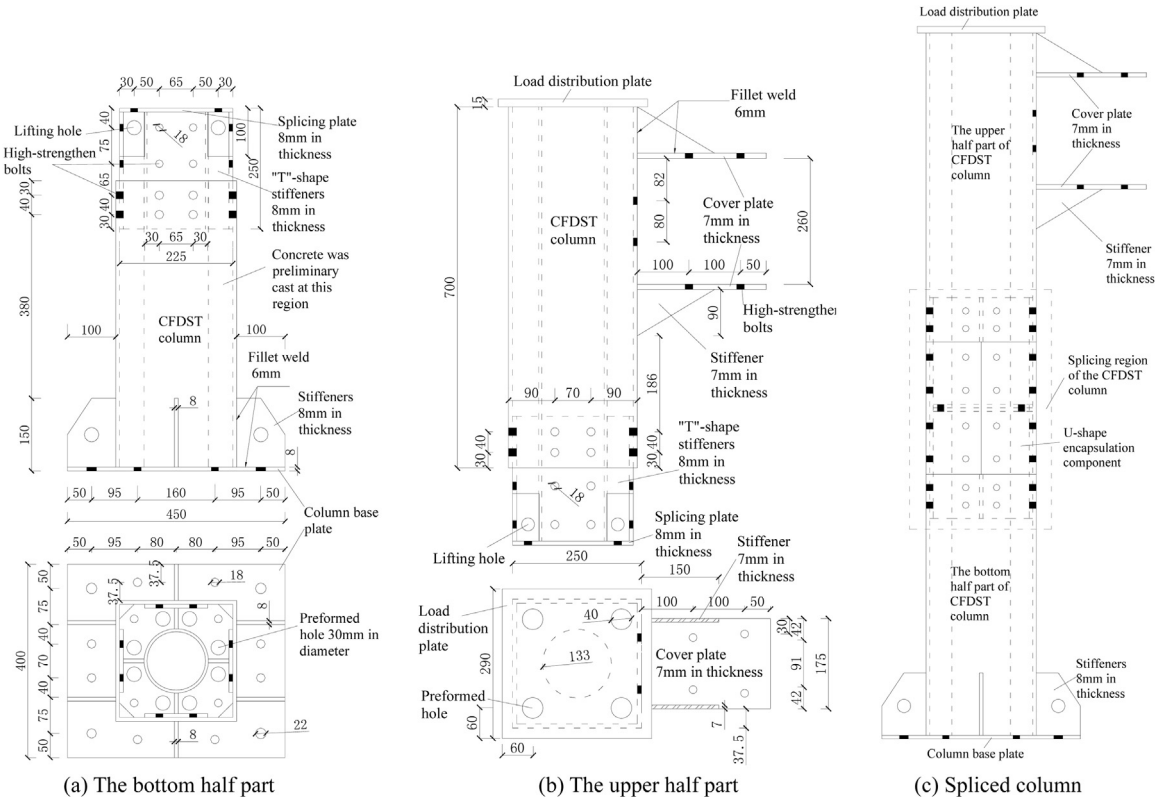

Fig. 2 – Dimensions of the splicing CFDST columns (unit: mm).

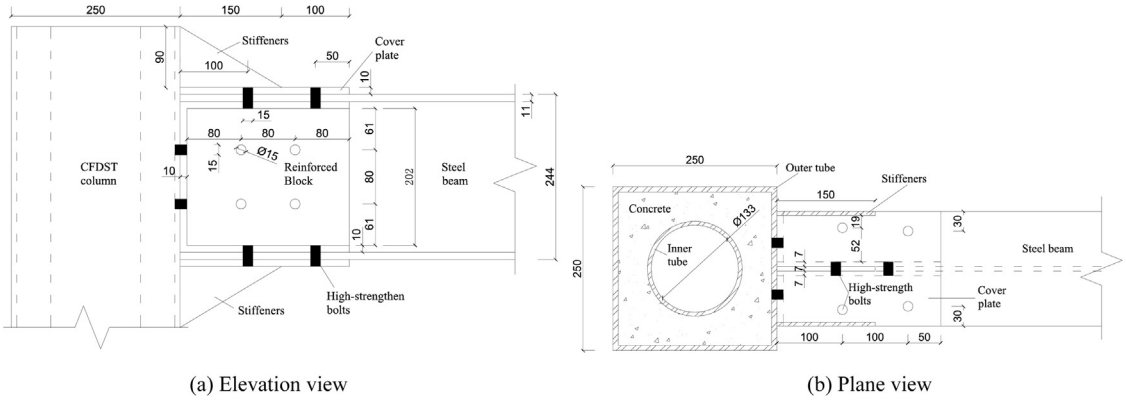

Fig. 3 – Dimensions of the beam-to-column connection (unit: mm).

mens were designed with different numbers of BRW, and they were labeled as BF-BRW-A (one piece of BRW) and BF-BRW-B (two pieces of BRW), and the detailed dimensions of these RC shear walls are presented in Fig. 5. The detailed dimensions of these specimens are presented in Table 1. The thickness of these walls was 60 mm, the thickness of concrete cover was 20 mm. Both of the plan size and thickness of these walls were reduced due to the 1/2-scaled size of the specimens. The diameter of the reinforcement bars was 5 mm, and the bars were two layers and were placed along two directions. The diameter of the high-strength bolts was 16 mm and the diameter of the bolt hole was 18 mm. The boundary frame of these shear walls were same with the BF specimen.

2.3. *Test setup*

Fig. 6 shows the diagram of the test setup and the photograph is shown in Fig. 7. Both of the lateral load and the vertical load were subjected to the test specimens. The lateral load was imposed by a hydraulic actuator, and the vertical load was imposed by hydraulic jack. The test specimens were placed on the rigid base beam and the base beam was connected with the base platform. Two supports and two trapezoid beams were used to restrain the lateral and vertical displacement of the base beam, respectively. A loading block was placed between the actuator and the specimens to transfer the lateral load. Two pairs of rolling supports were placed to restrain the

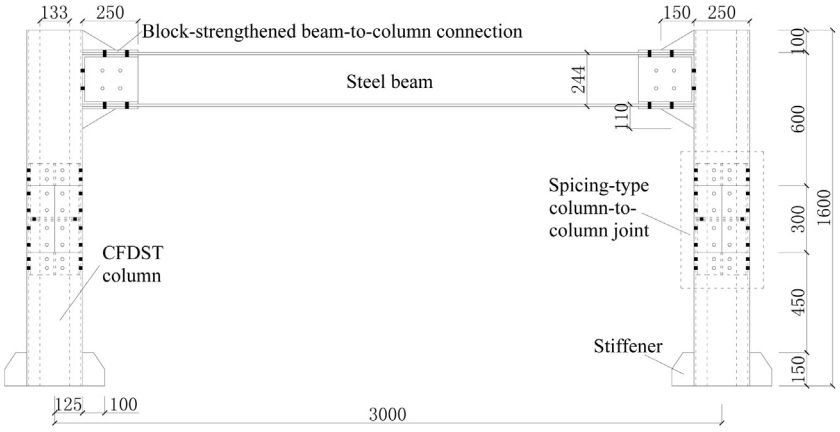

Fig. 4 – Dimensions of CFDST frame (BF, unit: mm).

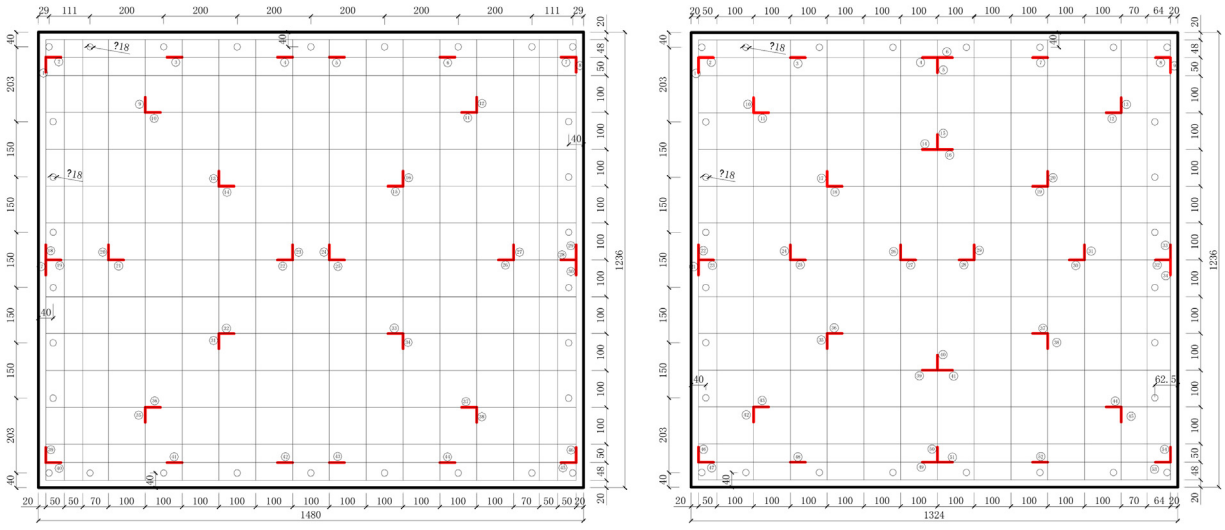

Fig. 5 – Dimensions and measuring points of the RC shear walls.

Table 1 – Dimensions of the specimens.

Specimen	CFDST frame (mm)	Number of SPW	Dimension of SPW (mm)
BF	CFDST column: 1600 (length), 250 (side length of outer tube) and 133	0	None
BF-BRW-A	(diameter of inner tube)	1	1480 (length) × 1236 (height)
BF-BRW-B	Beam: HM 244 × 175 × 7 × 11	2	1324 (length) × 1236 (height)

Note: 244 mm, 175 mm, 7 mm and 11 mm are the height, flange width, web thickness and flange thickness of the HM 244 × 175 × 7 × 11 beam.

out-of-plane deformation of the specimens during the loading stage, and such supports were connected with the lateral restraint beams, as shown in Fig. 7.

2.4. *Loading pattern and measurements*

The vertical load on each column was a constant load, and it was determined by the axial compression ratio of 0.5 and to represent the gravity loads from the above stories in the prototype building. The constant vertical load was applied on the CFDST columns preferentially and it was controlled by force. Then the cyclic lateral load was imposed on the right CFDST column by the actuator, and it was controlled by displacement. The controlled displacement loading pattern was determined by the Chinese standard JGJ 101-1996 [32], and a diagram of the loading pattern is shown in Fig. 8.

Both of the linear variable displacement transformers (LVDTs) and strain gauges were used to measure the deformation and stress distribution of the test specimens, respectively. The LVDTs measured the lateral displacement of the specimens, the shear deformation and the rotation deformation the beam-to-column joints, the lateral displacement of the base beam and the shear deformation of the RC shear walls. The lateral force of the specimens was

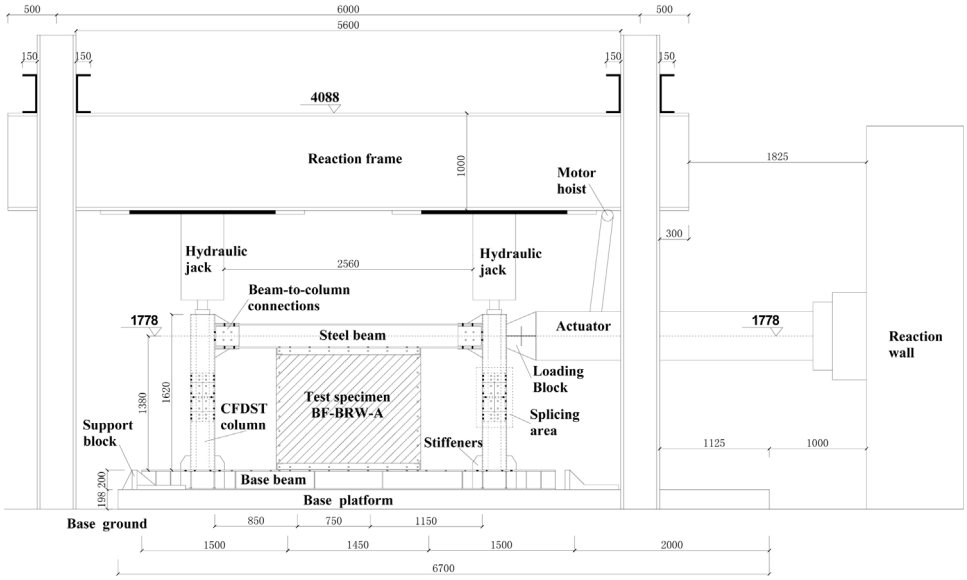

Fig. 6 – Test setup (unit: mm).

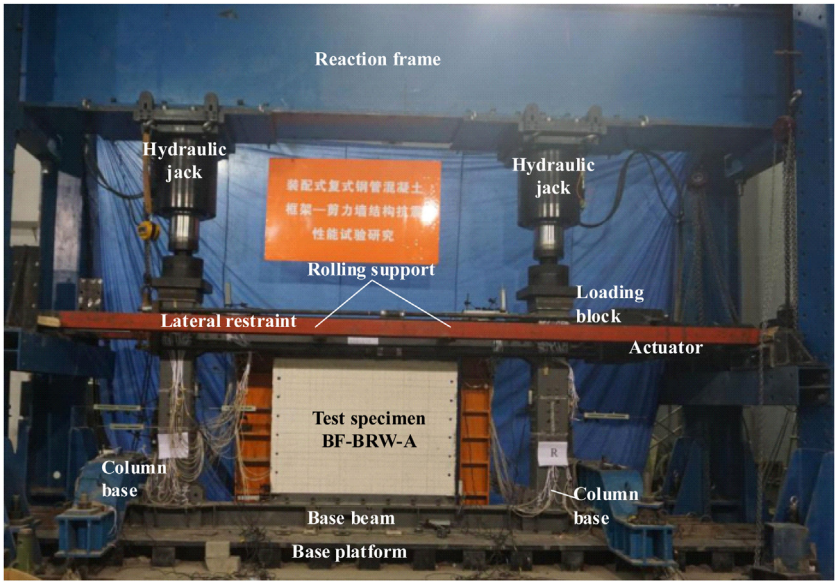

Fig. 7 – Diagram of the test specimens.

measured by the actuator. Several uniaxial strain gauges were used to record the stress distribution and stress transformation of the RC shear walls, and these gauges are depicted in Fig. 5.

2.5. *Mechanical properties of the materials*

The mechanical properties of the steel and concrete materials were determined by material tests. Three standard material test specimens were produced and were tested, and the average values of these results were selected to represent the material properties of these materials. Fig. 9 shows the dimensions of the standard material test specimens of steel, where b_0, L_0, L_c, r, D, H and C are 25 mm, 90 mm, 120 mm, 30 mm, 50 mm and 150 mm, respectively. The a_0 is the thickness of the standard material test specimens. The yield strength, elastic modulus and tensile strength of the steel members are shown in Table 2.

The compressive strength of the concrete material was measured by compressive testes on three standard 28-day proper-cured standard concrete cubes with 100 mm × 100 mm × 100 mm. The compressive strength of the concrete in CFDST columns and the RC shear walls were 24.5 MPa and 22.0 MPa. The tensile strength of the concrete in RC shear wall was 1.8 MPa. The pretension force of the frictional high-strength bolts was 100 kN, 155 kN and 490 kN for the grade levels of M16, M20 and M36, respectively. These bolts were designed as 10.9-grade, which means the yield strength and the yield strength ratio of these bolts were 1000 MPa and 0.9, respectively.

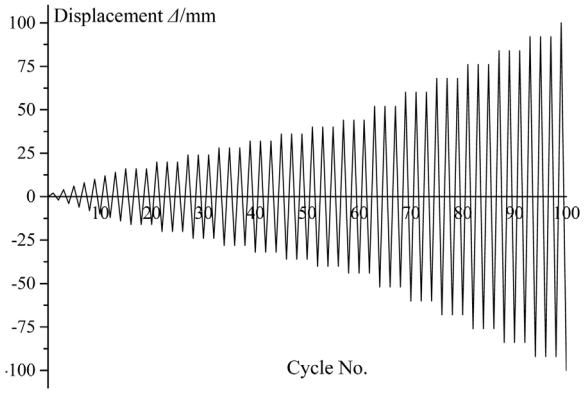

Fig. 8 – Loading rule of the test program.

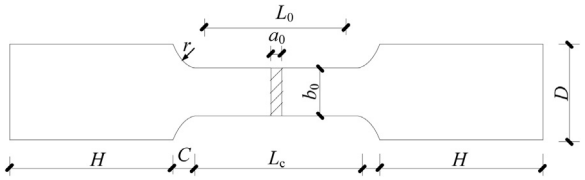

Fig. 9 – Dimensions of the standard samples for material test of steel.

3. Results of the test specimens

3.1. *Observed behavior of the specimens*

The failure mode of the BF specimen is presented in Fig. 10. Until 16 mm loading step, no obvious phenomenon was observed on the BF specimen, and it behaved in approximate elasticity. When the lateral drift reached 20 mm, noises were detected at the beam-to-column connections and the first crack was also detected on the weld between the stiffener and the CFDST column near by the beam-to-column connection. As the lateral drift reached 24 mm, more cracks formed on the welds between the stiffeners and the CFDST columns, and these cracks developed along the length of the welds. The stiffeners separated from the left CFDST column when the lateral load reached 60 mm, and obvious sliding deformation was detected at the beam-to-block connections. The stiffeners nearby the left column base buckled at this loading step. In the next loading step, the outer tube of the right CFDST column buckled, and the welds between the stiffeners and the CFDST columns nearby the column bases torn, as shown in Fig. 10(b) and (d). When the lateral drift reached 76 mm, the BF specimens failed with large plastic buckling deformation of CFDST column and strength degradation, as shown in Fig. 10(c) and (e). The final failure mode of the BF specimen is shown in Fig. 10(a).

The failure mode of the specimen BF-BRW-A is presented in Fig. 11. Minor cracks were observed on the RC shear wall when the lateral drift reached 4 mm, and these cracks were located at the four corners of the shear wall. The width of these cracks was no more than 0.5 mm and the length was no more than 10 cm. These cracks formed because the normal stress derived from bending moment exceeded the tensile strength of the concrete. These cracks developed steadily and some more minor cracks were formed at the end of the shear wall during the 6 mm loading step. Most of these cracks were developed along the horizontal direction and vertical direction. At the 8 mm loading step, an obvious diagonal crack was formed at the middle-bottom region and the width was 0.2 mm. Some cracks extended to the bottom of the shear wall, and the maximum length of these cracks was about 20 cm. The

Table 2 – Material properties of steel.

Items	Thickness or diameter	Yield strength f_y/MPa	Tensile strength f_u/Mpa	Elastic modulus E_s/Mpa
Outer tube	8	366.42	444.67	2.14×10^5
Inner tube	6	309.33	453.67	2.09×10^5
Beam flange	11	296.33	437.00	2.11×10^5
Beam web	7	280.33	421.33	2.08×10^5
Reinforcement bars	5	246.67	450.33	2.07×10^5

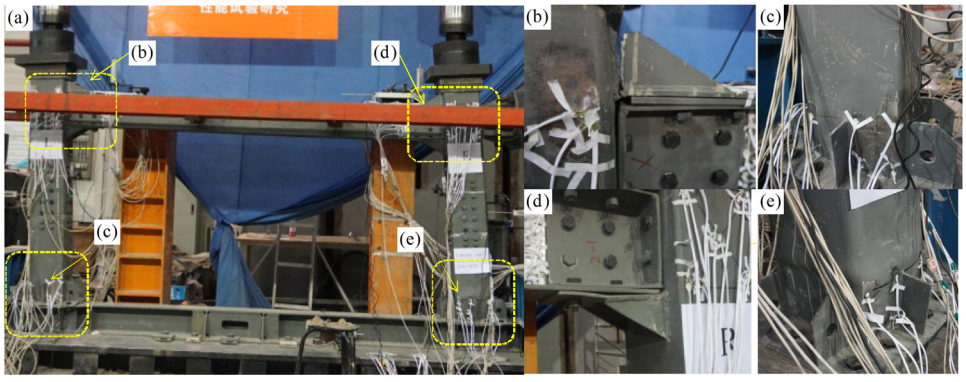

Fig. 10 – Failure patterns of the specimen BF (a. final failure mode; b. failure of the left beam-to-column joint; c. failure of the left CFDST column; c. failure of the right beam-to-column joint; c. failure of the right CFDST column).

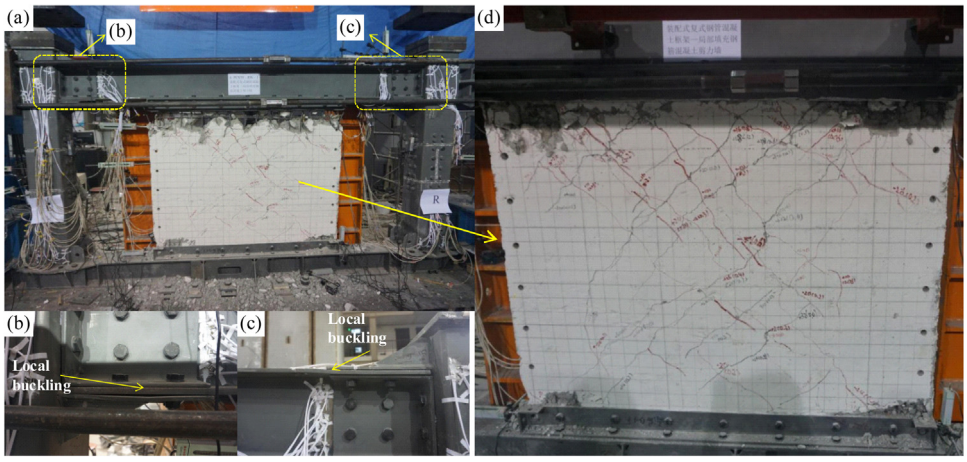

Fig. 11 – Failure patterns of the BF-BRW-A (a. finial failure mode; b. local buckling at the left beam-to-column joint; c. local buckling at the right beam-to-column joint; failure mode of the BRW-A).

diagonal cracks at the central position of the shear wall extended during the 10 mm loading step, and the width was 0.6 mm when the lateral drift reached 12 mm. The diagonal crack was formed because of the shear stress derived from shear force exceeded the shear strength of the concrete, and the angle of the diagonal crack was about 45°. The maximum length of the cracks reached 27 cm, but the width of these cracks was not increased so much. At the 14 mm loading step, a principal crack was formed at the upper-left corner of the shear wall nearby the angle, and the maximum width of the crack was 1.5 mm. In the negative loading stage of this loading step, another principal crack appeared at the right-top corner of the shear wall, and the width of the crack was 2.0 mm. More diagonal cracks appeared on the central region of the shear wall, and many cracks at the positions of the four corners developed into the central region. As the lateral drift reached 20 mm, minor spalls of the concrete were observed at the upper-right corner. The concrete crashed at the upper-left corner when the lateral drift was 24 mm, and then similar phenomenon appeared at the other corners of the shear walls at the next loading step. Due to the concrete crashed at the four corners, as shown in Fig. 11(d), the effective shear resisting section area of the shear wall was reduced, thus the maximum shear stress of the sections at the ends of the shear wall increased obviously. Cracks started to form at the central region of the upper and bottom sections, and these cracks developed quickly along with the strength degradation of the test specimen. Local buckling appeared at the cover plates and the steel beam due to the large bending moment derived from lateral force, as shown in Fig. 11(a) and Fig. 11(b), respectively. At the 36 mm loading step, the cracks at the four corners developed across the thickness direction of the shear wall, and reinforcement bars at these positions exposed obviously. Besides, cracks were formed on the welds in the beam-to-column connections. The capacity of the specimen decreased suddenly at the 40 mm loading step, straight-line joint failure was observed at the upper section of the RC shear wall, and the RC shear wall basically lost its capacity at this loading step. As the lateral drift was 52 mm, cracks were observed on the welds between the stiffeners and the CFDST column at the position of column bases, and these cracks developed along the welds. Local buckling then developed on the CFDST columns nearby the column bases, and the buckling developed quickly and obviously during 60 mm loading step. When the lateral drift was 68 mm, the welds between the stiffeners and the cover plates torn, and the plate of the CFDST columns nearby the stiffeners torn quickly. The test was terminated at the 76 mm loading step due to large strength degradation of the specimen, and the final failure mode of the BF-BRW-A is shown in Fig. 11(a).

The failure mode of the specimen BF-BRW-B is presented in Fig. 12. There were two pieces of BRW in the specimen BF-BRW-B, which was different with the specimen BF-BRW-A. When the lateral drift was 4 mm, some minor cracks appeared on the upper-right corner of the left BRW and the upper-left corner of the right BRW, the thickness and the length of these cracks were no more than 0.28 mm and 20 cm, respectively. At the 6 mm loading step, cracks were formed on the corners of the BRWs because of the action of the normal stress. As like the specimen BF-BRW-A, these cracks developed steadily along the vertical and the horizontal directions. Besides, diagonal cracks were formed at the central region of the BRWs at this loading step. These diagonal cracks developed, and the maximum one was about 10 cm in length when the lateral drift was 10 mm. The maximum width and length of the cracks at the corners were about 0.7 mm and 40 cm, respectively. These cracks extended during from the 12 mm to the 20 mm loading step. When the lateral drift reached 24 mm, the concrete at the upper-left of the left BRW and the right BRW crashed, and the specimen reached its ultimate capacity. Then the cracks extended to the ends of the shear walls, and the maximum length of the cracks was about 58 cm. The cracks started to extend along the upper and bottom sections of the BRWs, especially for the right BRW, which resulted strength degradation of the specimen. The right BRW almost lost its capacity due to straight-line joint failure at the upper section during the 40 mm loading step, and the capacity of the specimen reached a lower peak value when the lateral drift was 44 mm, as shown in Fig. 12(d). The flange plate of the steel beam and the cover plate buckled at this loading step, as shown in Fig. 12(b) and (c). The

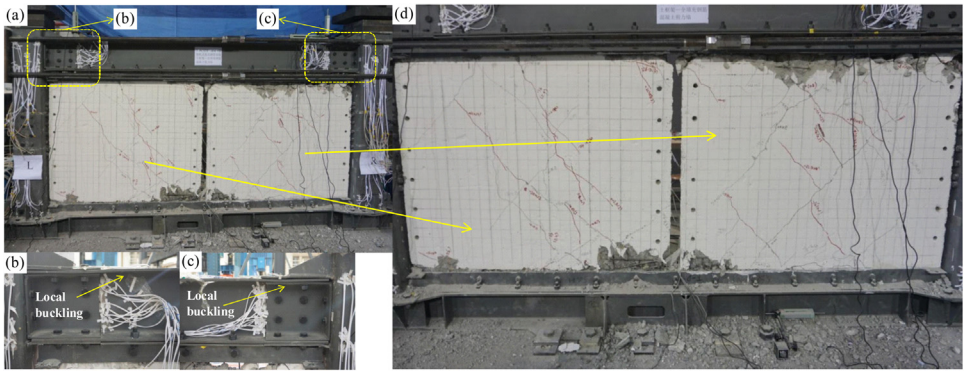

Fig. 12 – Failure characteristics of the specimen BF-BRW-B (a. finial failure mode; b. local buckling at the left beam-to-column joint; c. local buckling at the right beam-to-column joint; failure mode of two piece of BRW-Bs).

left BRW still supplied lateral resistance during the 52 mm and 60 mm loading steps, and the capacity of the specimen slightly increased. But the specimen reached its ultimate capacity when the lateral drift was 60 mm, large area of concrete crashed and the weld between the stiffeners and the CFDST columns torn. Local buckling occurred at the steel plates of the CFDST columns nearby the column bases, both of the left BRW and the right BRW separated from the boundary frame. The capacity of the specimen decreased sharply due to the failure of the BRWs and the CFDST frames. The welds between the stiffeners and the CFDST columns nearby the column base and the welds between the cover plates and the CFDST column torn, and the plastic deformation derived from local buckling of the column bases developed obviously. The test of the specimen BF-BRW-B was terminated at the 84 mm loading step, and the final failure mode of the BF-BRW-B is shown in Fig. 12(a).

3.2. *Load–displacement curves*

The hysteretic curves and the envelop curves of the specimens are shown in Fig. 13. It can be found that all specimens exhibit good performance and deformation capacity. Both of the initial stiffness and the ultimate capacity of the CFDST frames were enhanced by the beam-only-connected precast RC shear walls. The shuttle shape of the hysteretic curve of the BF specimen indicates that this specimen has good ductility and energy dissipation capacity. Two obvious stages can be observed in Fig. 13(b), the lateral resistance decreased suddenly when the lateral drift reached 40 mm. Because the RC shear wall failed at this loading step, and the boundary frame supplied the lateral resistance, thus the hysteretic curve of the BF-BSW-A during 44–76 mm was similar with the one in BF Specimen. But for the specimen BF-BSW-B, three obvious stages were observed. The lateral resistance suddenly decreased when the lateral drift reached 44 mm, and it increased during 52 mm to 60 mm. Then the lateral resistance of the BF-BRW-B decreased sharply after 60 mm loading step.

The lateral loads, lateral drift, initial stiffness and displacement-based ductility ratio of the test specimens at the yield point and ultimate point are shown in Table 3. The initial stiffness is selected as the slope of the envelop curves at the first loading step (2 mm). The average stiffness of the BF-BRW-A and the BF-BRW-B enhanced 25.95 kN/mm (50.8%) and 57.59 kN/mm (58.7%) by comparing with the value for the BF, respectively. The average lateral resistance of the BF-BRW-A and the BF-BRW-B enhanced 188.72 kN (33.4%) and 331.88 kN (58.7%) by comparing with the value for the BF, respectively. These specimens tolerated more than 4% inter-story drift ratio and still exhibited considerable loading capacity, and 4% is limitation inter-story drift ratio of the collapse prevention (CP) performance level in FEMA 356 [34] for steel-moment resisting frame structures. FEMA 356 is a guidance for performance-based seismic design of building structures in Unite States, and the performance levels are proposed to define the damage states of building structures. Besides, the deformation capacity of the test specimens is also larger than the limitation value (2%) for steel structures subjected to rare earthquake in the Chinese standard GB 50011-2010 [35]. The ductility ratio is calculated as the ratio of yield displacement to the maximum displacement. The yield displacement is determined by the equal-energy methodology proposed in literature [25], which is the most commonly used method to determine the yield point of cyclic test specimens, the detailed diagram of the method is shown in Fig. 14. The maximum displacement is determined as the displacement of the specimens when the lateral load degraded to 85% of the ultimate values [32]. The average ductility ratio of the BF-BRW-B is slight larger than the value of the specimen BF, however, the value for the BF-BRW-A is less than the value for other two. Because there was a sudden degradation on lateral capacity of the BF-BRW-A due to the sudden failure of the BRW.

3.3. *Stiffness and strength degradation*

The secant stiffness K curve is used to present the stiffness degradation of the test specimens in the loading process, and reflects the whole damage process of the test specimens. The secant stiffness can be calculated by

$$K_i = \frac{|+P_i| + |-P_i|}{|+\Delta_i| + |-\Delta_i|} \tag{1}$$

where K_i is the secant stiffness of the specimens at the ith loading step; $+P_i$ and $-P_i$ are the peak load at the ith positive and negative loading steps, respectively; $+\Delta_i$ and $-\Delta_i$ are the corresponding displacement at the ith positive and negative loading steps, respectively.

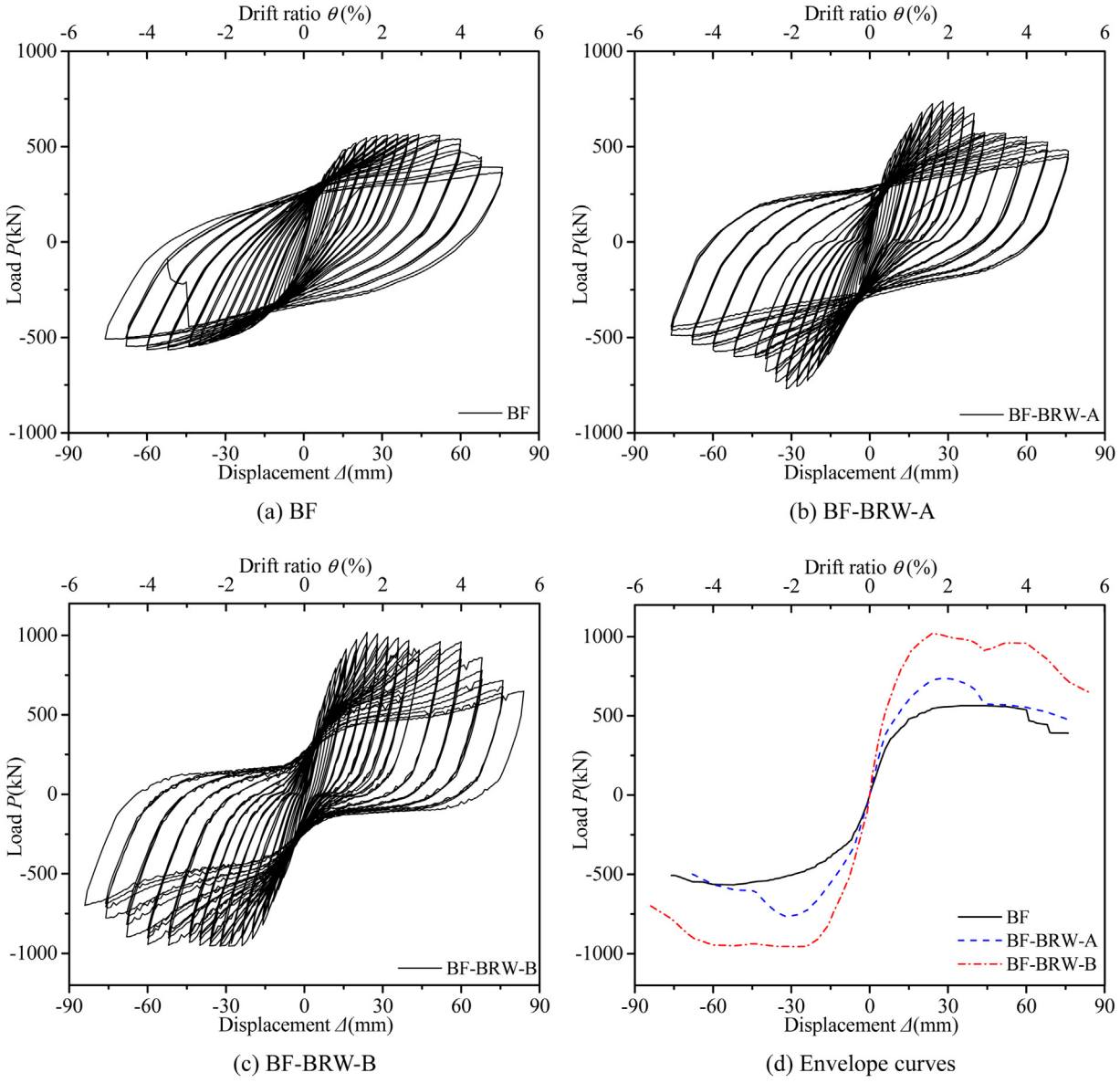

Fig. 13 – Load versus displacement curves for the test specimens.

Table 3 – Results of some key points of the test specimens.

Specimen	Direction	Yield			Maximum			Ductility ratio $\mu = \Delta_{max}/\Delta_y$	Elastic stiffness K_e (kN/mm)
		P_y (kN)	Δ_y (mm)	φ_y (%)	P_{max} (kN)	Δ_{max} (mm)	φ_{max} (%)		
BF	Positive	479.13	15.11	1.01	564.34	60.88	4.06	4.03	51.55
	Negative	−425.79	−18.67	1.24	−565.50	−76.00	5.07	4.07	50.58
BF-BRW-A	Positive	618.58	15.92	1.06	739.06	41.65	2.78	2.62	80.25
	Negative	−583.61	−16.32	1.09	−768.22	−41.44	2.76	2.53	73.79
BF-BRW-B	Positive	906.44	15.80	1.05	1018.62	67.12	4.47	4.26	114.48
	Negative	−860.76	−17.52	1.17	−954.33	−73.92	4.93	4.21	102.84

Note: P_y and P_{max} are the yield load and the ultimate capacity, respectively; Δ_y and Δ_{max} are the yield drift and the maximum drift, and the φ_y and φ_{max} are the corresponding drift ratio, respectively; K_e is the initial lateral stiffness.

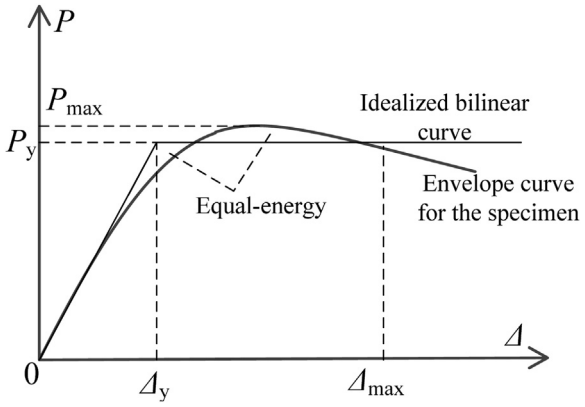

Fig. 14 – Diagram for determining yield point.

The secant stiffness curve of the test specimens is shown in Fig. 15(a). It can be found that the BF-BRW-B exhibits largest secant stiffness in the whole loading process, and the value of the BF-BRW-A is lower than the value of BF-BRW-B but larger than the value of BF. The results indicate that the BRWs could effectively enhance the lateral stiffness of the CFDST frames in the whole loading process, and the lateral stiffness of the CFDST frames could be efficiently enhanced by increasing the amount of BRWs, which is also demonstrating the good cooperative working relationship between CFDST frames and BRWs. For the BF-BRW-A, the enhancement on secant stiffness by comparing with the BF is diminished when the lateral drift reached 44 mm, because the BRW damaged seriously at the 40 mm loading step.

The strength degradation coefficient λ is used to present the strength degradation behavior of the test specimens due to cyclic loads at the same level of lateral loads, such coefficient could reflect the stability of lateral resistance of the test specimens subjected to cyclic loads. The calculation of the coefficient is

$$\lambda_{ij} = \frac{P_j^{i+1}}{P_j} \tag{2}$$

where λ_{ij} is the strength degradation coefficient of the specimens at the jth loading level subjected to ith loading cycle, P_j^{i+1} is the peak load of the specimens at the jth loading level subjected to $(i+1)$th loading cycle, P_j is the peak load of the specimens at the jth loading level subjected to first loading cycle.

The strength degradation coefficient of the test specimens is shown in Fig. 15(b). The coefficients of the specimens are larger than 0.85 and most of them are larger than 0.95, indicating that lateral resistance of the CFDST frame and CFDST frame with beam-only-connected BRW structures is stable subjected to cyclic loads. Generally, the coefficients decrease with increasing of the lateral drift. In the early loading stages (lateral drift is less than 32 mm), the BF exhibits the highest coefficients, and the values of the BF-BRW-A are higher than the values of BF-BRW-B. Because the BRW damaged successively in the early loading stages, and such damages would result in strength degradation of the specimens, especially for the BF-BRW-B. There is a sharp degradation for BF-BRW-A when the lateral drift was 40 mm, because the BRW damaged seriously at this loading step. Then the coefficient of BF-BRW-A is similar with the value of BF because the BRW was almost destroyed at the following loading steps. But for BF-BRW-A, no sharp degradation was occurred because two pieces of BRWs were placed and the damage process of the BRWs was slowly.

3.4. *Ultimate capacity of the BRW members*

According to the suggestion by Jiang et al. [25], the ultimate capacity of the BF-BRWs can be simplified as the sum of the capacities of the BF and the infilled BRWs. Such simplified method was verified by cyclic tests on four specimens conducted by Jiang et al. [25]. Thus the ultimate capacity of the BF-BRWs can be calculated by

$$V = V_f + V_w = V_f + sum(V_{wi}, i = 1, 2, \ldots) \tag{3}$$

where V_f is the capacity of the bare frame, V_w is the total capacity sum of the BRWs and V_{wi} is the capacity of the ith BRW.

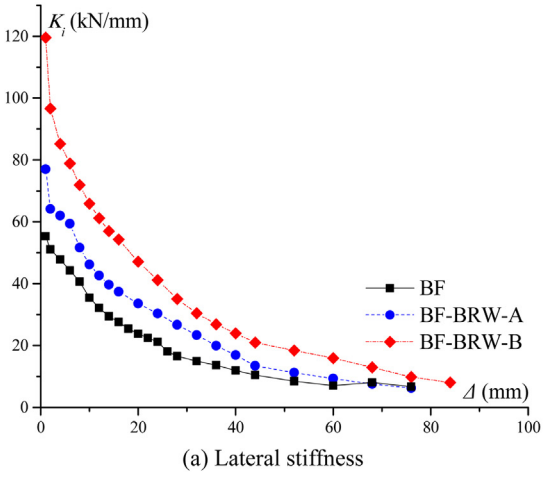

(a) Lateral stiffness

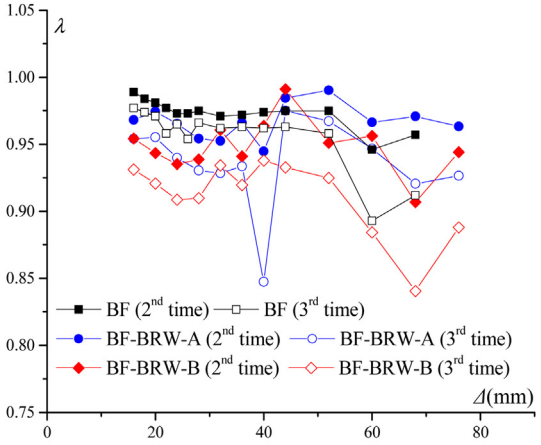

(b) Lateral strength

Fig. 15 – Degradation curves of the test specimens.

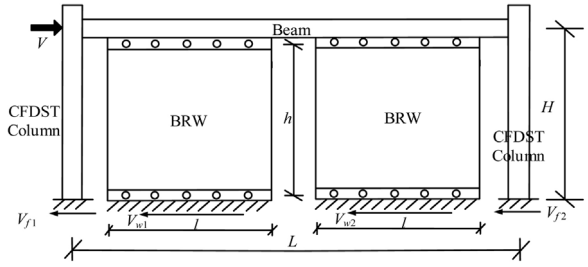

Fig. 16 – Mechanical diagram of the BF-BRW-B.

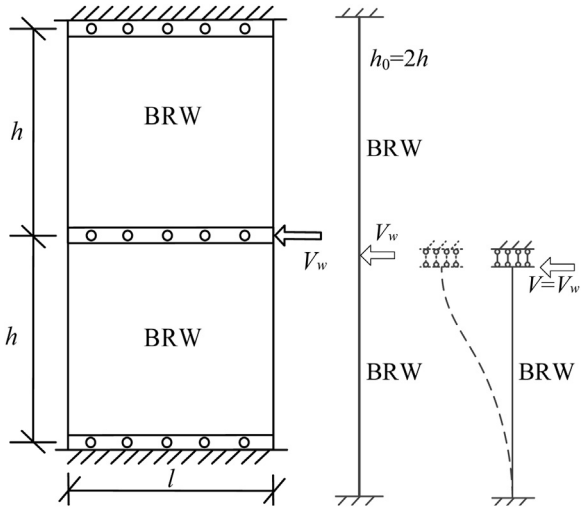

Fig. 17 – Diagram of the deep beam model.

The capacity of the CFDST frame has been investigated [18], the interaction relation of the axial force, bending moment and shear force is considered, and the capacity was also verified by the test results. In this paper, only the ultimate capacity of the BRWs in the specimens is calculated. Taking the specimen BF-BRW-B for example, the mechanical diagram is depicted in Fig. 16. The V_{w1} and V_{w2} are the shear force of the left BRW and the right BRW, respectively; V_{f1} and V_{f2} are the shear force of the left column and the right column, respectively.

The height-to-length ratio ($2h/l$) is 1.61 and 1.78 for the BRW in the BF-BRW-A and the BF-BRW-B, respectively. Due to the length-to-height ratio of these BRWs is less than 2.0, thus the BRWs can be considered as a deep beam based on the Chinese Standard GB 50010-2010 [33], which is a standard for designing of reinforced concrete structures. The deep beam model is used to predict the lateral resistance of the BRWs, because the bend-shear mechanical behavior of the BRWs is similar with a fixed deep beam. Thus two BRWs can be simplified a fixed deep beam, as shown in Fig. 17, and the lateral resistance of a BRW can be calculated as half of the resistance of the deep beam subjected to a concentrated load.

The ultimate capacity of a deep beam subjected to a concentrated load can be calculated by

$$V_{wu} = P_{mu} = \frac{1.75}{\lambda + 1.0} f_t b l_0 + \frac{(h_0/l-2)}{3} f_{yv} \frac{A_{sv}}{s_h} l_0 + \frac{(5-h_0/l)}{6} f_{yh} \frac{A_{sh}}{s_v} l_0 \quad (4)$$

where λ is the shear-span ratio of the assumed deep beam, and it is 0.25 due to the $h_0/l \le 2.0$; h_0/l is the length-to-height ratio of the assumed deep beam, and it is defined as 3.0 due to the $h_0/l < 2.0$; α_s is the cover thickness of the BRW; l and l_0 ($l_0 = l - 2\alpha_s$) are the length of the BRWs and effective height of the assumed deep beam, respectively; h and h_0 is the effective height of the BRWs and the effective length of the assumed deep beam; f_t is the tensile strength of concrete; f_{yv} and f_{yh} are the yield strength of the reinforcement bars along the vertical and horizontal directions, respectively; A_{sv}/s_h and A_{sh}/s_v are the stirrup ratio of the reinforcement bars along the vertical and horizontal directions, respectively.

Thus the ultimate capacity of the BRWs in the specimens BF-BRW-A and the BF-BRW-B can be calculated according to Eq. (4), and the predicted results as well as the test results are compared in Table 4. Where the V_{pre} and the V_{exp} are the predicted ultimate capacity and the ultimate capacity obtained from the test, respectively. Due to the specimen BF-BRW-B has two pieces of BRW, thus the V_{pre} is determined as two times of the ultimate capacity of BRW-B. It can be found that the maximum error between the predicted and the test results is 14.7%, and the predicted ultimate capacity of the BRWs in the test specimens is larger than the test result. Because the bolt connections between the BRW and the steel beam (wall-to-frame bolt connections) damaged during the tests, which resulted in reduction on the ultimate capacity of the test specimens.

4. Conclusion

This paper presents experimental investigations on the concrete-filled double-skin steel tube/moment-resisting frames with beam-only-connected precast reinforced concrete shear walls, three large scale specimens were tested and compared, the conclusions are:

(1) The main failure mode of the beam-only-connected precast reinforcement concrete shear walls (BRW) was shear-bending failure based on the experimental observation. Cracks were firstly formed at the four corners and the central region of the BRWs due to the normal stress and the

Table 4 – Comparison on ultimate capacities of the predicted and the test results.

Member	l (mm)	h_0 (mm)	l_0 (mm)	λ	A_{sv}/s_h (mm²/m)	A_{sh}/s_v (mm²/m)	V_{pre} (kN)	V_{exp} (kN)	V_{pre}/V_{exp}
BRW-A	1480	2380	1440	0.25	2.01	1.63	226.0	202.72	1.115
BRW-B	1340	2380	1300	0.25	1.88	1.63	260.0 (one) 519.9 (two)	453.12	1.147

shear force derived from bending moment and shear force, respectively. Then, the concrete at the four corners crashed due to the action of the bending moment, and the effective section area of the section at the ends of the BRWs decreased successively. Lastly, the BRW failed due to reduced section area and increased shear force.

(2) The BRWs significant enhanced the initial stiffness and ultimate capacity of the CFDST frame. The increments on initial stiffness were 25.95 kN/mm (50.8%) and 57.59 kN/mm (58.7%) of the BF-BRW-A and the BF-BRW-B, respectively. The increments on ultimate capacity were 188.72 kN (33.4%) and 331.88 kN (58.7%) of the BF-BRW-A and the BF-BRW-B, respectively. It is indicated that the proposed beam-only-connected precast RC shear walls and the proposed frame-to-wall bolt connections are effective to strengthen the CFDST frames.

(3) The ultimate inter-story drift of the test specimens was larger than 4.0%, which is larger than the limited value of steel structures subjected to rare earthquake (2%) in the Chinese Standard GB 50011-2010 [35] and collapse prevention (CP) performance limit (4%) of steel moment-resisting frame structures in FEMA 356 [34]. It is demonstrating that the proposed fully-prefabricated structural system exhibits good ability in lateral deformation and suitable for high-rise buildings in earthquake regions.

(4) This paper suggested that the BRW could be design by estimated deep beam model, and the formula on the capacity calculation of fixed RC deep beam in the Chinese standard GB 50010-2010 [33] was proposed to predict the ultimate capacity of the BRW. The predicted results were also validated by the test results, the maximum error was no more than 14.7%.

It should be highlighted that the qualitative data presented in this paper are derived from the limited numbers of specimens. But the presented data are the sole validation test data for the proposed system in the current knowledge. The authors would conduct further analytical study to reach more general results, which could be used for seismic design of the proposed system.

Conflict of interest

None declared.

Ethical statement

Authors state that the research was conducted according to ethical standards.

Acknowledgement

This work was sponsored by the National Natural Science Foundation of China (51878056) and the Fundamental Research Funds for the Central Universities, CHD (300102288703) and the Social Development Foundation for Science and Technology Planning Project of Shaanxi Province (2019SF-256).

REFERENCES

[1] L.H. Han, W. Li, R. Bjorhovde, Developments and advanced applications of concrete-filled steel tubular (CFST) structures: members, Journal of Constructional Steel Research 100 (2014) 211–228.

[2] L.H. Han, H. Huang, Z. Tao, X.L. Zhao, Concrete-filled double skin steel tubular (CFDST) beam-columns subjected to cyclic bending, Engineering Structures 28 (12) (2006) 1698–1714.

[3] Y.F. Zhang, J.H. Zhao, W.F. Yuan, Study on compressive bearing capacity of concrete-filled square steel tube column reinforced by circular steel tube inside, Journal of Civil Engineering and Management 19 (2013) 787–795.

[4] M.F. Hassanein, O.F. Kharoob, L. Gardner, Behavior and design of square concrete-filled double skin tubular columns with inner circular tubes, Engineering Structures 100 (2015) 410–424.

[5] Y.H. Wang, G.B. Lu, X.H. Zhou, Experimental study of the cyclic behavior of concrete-filled double skin steel tube columns subjected to pure torsion, Thin-walled Structures 122 (2018) 425–438.

[6] K. Uenaka, Concrete filled double skin tubular deep beam having outer circular and inner square sections under bending-shear, Structures 14 (2018) 313–321.

[7] M. Ahmed, Q.Q. Liang, V.I. Patel, M.N.S. Hadi, Nonlinear analysis of rectangular concrete-filled double steel tubular short columns incorporating local buckling, Engineering Structures 175 (2018) 13–26.

[8] L.H. Han, W.D. Wang, X.L. Zhao, Behaviour of steel beam to concrete-filled SHS column frames: finite element model and verifications, Engineering Structures 30 (2008) 1647–1658.

[9] K.C. Tsai, P.C. Hsiao, K.J. Wang, Y.T. Weng, M.L. Lin, K.C. Lin, C.H. Chen, J.W. Lai, S.L. Lin, Pseudo-dynamic tests of a full-scale CFT/BRB frame—Part I: Specimen design, experiment and analysis, Earthquake Engineering and Structural Dynamic 37 (7) (2008) 1081–1098.

[10] J.M. Castro, A.Y. Elghazouli, B.A. Izzuddin, Modeling of the panel zone in steel and composite moment frames, Engineering Structures 27 (2013) 129–144.

[11] K.A. Skalomenos, G.D. Hatzigeorgiou, D.E. Beskos, Modeling level selection for seismic analysis of concrete-filled steel tube/moment-resisting frames by using fragility curves, Earthquakes Engineering and Structural Dynamics 44 (2015) 199–220.

[12] J.F. Wang, J.X. Wang, H.T. Wang, Seismic behavior of blind bolted CFST frames with semi-rigid connections, Structures 9 (2017) 91–104.

[13] F.X. Ding, G.A. Yin, L.Z. Jiang, Y. Bai, Composite frame of circular CFST column to steel–concrete composite beam under lateral cyclic loading, Thin-walled Structures 122 (2018) 137–146.

[14] L.H. Guo, R. Li, S.M. Zhang, Cyclic behavior of SPSW and CSPSW in composite frame, Thin-walled Structures 51 (2012) 39–52.

[15] Y.F. Zhang, J.H. Zhao, C.S. Cai, Seismic behavior of ring beam joints between concrete-filled twin steel tubes columns and reinforced concrete beams, Engineering Structures 39 (2012) 1–10.

[16] Y.F. Zhang, D.F. Zhang, Experimental study on the seismic behaviour of the connection between concrete-filled twin steel tubes column and steel beam, European Journal of Environmental and Civil Engineering 19 (3) (2015) 347–365.

[17] Y. Hu, J.H. Zhao, D.F. Zhang, Y.F. Zhang, Seismic risk assessment of concrete-filled double-skin steel tube/

moment-resisting frames, Earthquakes and Structures 14 (3) (2018) 249–259.
[18] Y. Hu, J.H. Zhao, D.F. Zhang, C. Chen, Experimental seismic performance of concrete-filled double-skin steel tube moment-resisting frames with different construction details, Journal of Constructional Steel Research (2018) (under review).
[19] J.H. Ye, L.Q. Jiang, Collapse mechanism analysis of a steel moment frame based on structural vulnerability theory, Archives of Civil and Mechanical Engineering 18 (3) (2018) 833–843.
[20] A. Dall'Asta, G. Leoni, F. Morelli, W. Salvatore, A. Zona, An innovative seismic-resistant steel frame with reinforced concrete infill walls, Engineering Structures 141 (2017) 144–158.
[21] S.J. Hashemi, J. Razzaghi, A.S. Moghadam, P.B. Lourenco, Cyclic testing of steel frames infilled with concrete sandwich panels, Archives of Civil and Mechanical Engineering 18 (2) (2018) 557–572.
[22] G.H. Sun, Q. Gu, Q.C. Li, Y.Z. Fang, Experimental and numerical study on the hysteretic behavior of composite partially restrained steel frame-reinforced concrete infill walls with vertical slits, Bulletin of Earthquake Engineering 16 (3) (2018) 1245–1272.
[23] B. Qu, M. Bruneau, Design of steel plate shear walls considering boundary frame moment resisting action, Journal of Structural Engineering 135 (2009) 1511–1521.
[24] P.M. Clayton, J.W. Berman, L.N. Lowes, Seismic performance of self-centering steel plate shear walls with beam-only-connected web plates, Journal of Constructional Steel Research 106 (2015) 198–208.
[25] L.Q. Jiang, H. Zheng, Y. Hu, Experimental seismic performance of steel- and composite steel-panel wall strengthened steel frames, Archives of Civil and Mechanical Engineering 17 (3) (2017) 520–534.
[26] R.S. Ju, H.J. Lee, C.C. Chen, C.C. Tao, Experimental study on separating reinforced concrete infill walls from steel moment frames, Journal of Constructional Steel Research 71 (4) (2012) 119–128.
[27] L.Q. Jiang, H. Zheng, Y. Hu, Seismic behaviour of a steel frame partially infilled with precast reinforced concrete wall, Advances in Structural Engineering 19 (10) (2016) 1637–1649.
[28] Y. Ozcelik, P.M. Clayton, Behavior of columns of steel plate shear walls with beam-connected web plates, Engineering Structures 172 (2018) 820–832.
[29] B. Shekastehband, A.A. Azaraxsh, H. Showkati, Experimental and numerical study on seismic behavior of LYS and HYS steel plate shear walls connected to frame beams only, Archives of Civil and Mechanical Engineering 17 (2017) 154–168.
[30] L.H. Guo, Q. Rong, B. Qu, J.P. Liu, Testing of steel plate shear walls with composite columns and infill plates connected to beams only, Engineering Structures 136 (2017) 165–179.
[31] L.Q. Jiang, H. Zheng, Y. Hu, Effects of various uncertainties on seismic risk of steel frame equipped with steel panel wall, Bulletin of Earthquake Engineering 16 (12) (2018) 5995–6012.
[32] JGJ 101, Specification of Testing Methods for Earthquake Resistant Building, Chinese Architecture & Building Press, Beijing, China, 1996.
[33] GB 50010, Code for Design for Concrete Structures, Architecture & Building Press, China, 2010.
[34] FEMA 356, NEHRP Guidelines for the Seismic Rehabilitation of Buildings, Federal Emergency Management Agency, Washington (DC), 2000.
[35] GB 50011, Code for Seismic Design of Buildings, Chinese Architecture & Building Press, Beijing, China, 2010.